



## Short Communication

# Flexible naphthalene-based polyimide nanofiber cathode with hierarchical micro/nanoporous structure for high-performance organic sodium-ion batteries

Gangyong Zhou<sup>a</sup>, Lulu Mo<sup>a</sup>, Chunyang Zhou<sup>a</sup>, Yan Lv<sup>a,\*\*\*</sup>, Yue-E Miao<sup>a,\*</sup>, Tianxi Liu<sup>a,b,\*\*</sup>

<sup>a</sup> State Key Laboratory for Modification of Chemical Fibers and Polymer Materials, College of Materials Science and Engineering, Innovation Center for Textile Science and Technology, Donghua University, Shanghai 201620, PR China

<sup>b</sup> Key Laboratory of Synthetic and Biological Colloids, Ministry of Education, School of Chemical and Material Engineering, Jiangnan University, Wuxi 214122, PR China



## ARTICLE INFO

## Keywords:

Polyimide nanofiber cathode  
Electrospinning  
Hierarchical micro/nanoporous structure  
Organic sodium-ion batteries

## ABSTRACT

A flexible composite nanofibrous organic cathode, consisting of naphthalene-based polyimide/nitrogen-doped carbon/carbon nanotubes (NPI/NC/CNT) with hierarchical micro/nanoporous structure, is designed for sodium-ion batteries (SIBs). The in-situ formed three-dimensional conductive network can achieve a uniform distribution and increased interfacial contact between electroactive NPI and electrolyte, thereby leading to high utilization of NPI. As a result, the free-standing NPI/NC/CNT cathode delivers high reversible capacity, superior rate capability, and excellent cycling stability for SIBs.

## 1. Introduction

Benefitting from the abundant resources and environmental friendliness of sodium, exploiting advanced rechargeable sodium-ion batteries (SIBs) to replace conventional lithium-ion batteries (LIBs) is of great significance to alleviate the scarcity and uneven distribution of lithium resources [1–4]. Tremendous efforts have been made in SIB electrode materials, which however are still suffered from the low specific capacity and poor cycle life because of the intrinsic large ionic radius of sodium and sluggish reaction kinetics [1,5–10]. Among various electrode materials, electroactive organic compounds have been considered as the most promising choices for SIBs because of the nearly inexhaustible resources, environmental benignity and structure versatility [11–14]. Especially, organic electrode materials possess good tolerance for the larger Na<sup>+</sup> radius and tunable electrochemistry compared with their inorganic counterparts due to the storage mechanism of chemical bond reactions [14–16]. Typically, organic carbonyl compounds are being widely investigated as cathode materials for SIBs due to plenty of electroactive functional groups (C=O) and tunable redox potentials [17–19]. As one of the typical conjugated carbonyl compounds, 1,4,5,8-naphthalenetetracarboxylic dianhydride (NTCDA) has attracted

increasing attentions as cathode materials for Na storage owing to its high theoretical capacity and tailorable electrochemical properties [20–23]. However, the small molecule of NTCDA exhibits drastic capacity fading and inferior rate performance due to its critical dissolution in electrolytes and poor conductivity. To address these issues, the combination of molecular polymerization and synthesis of carbonaceous composites is supposed as an effective approach to suppress the solubility of NTCDA in electrolytes and enhance its conductivity [24,25]. Although mitigated dissolution and enhanced conductivity of naphthalene-based cathode materials can be achieved using the above strategy, the sluggish reaction kinetics and low utilization of electroactive functional groups still remain challenge due to the agglomeration of powdery structure and polymer binder usage. Moreover, using metal current collector will reduce the energy density of electrode materials. Therefore, it is of vital importance to develop free-standing naphthalene-based cathode with stable structure, superior conductivity and ultrafast reaction kinetics for SIBs.

Herein, we report a flexible naphthalene-based polyimide nanofiber composite electrode with hierarchical micro/nanoporous structures through a simple electrospinning technique and heat treatment as illustrated in Fig. 1a. The composite electrode, consisting of

\* Corresponding author.

\*\* Corresponding author. Key Laboratory of Synthetic and Biological Colloids, Ministry of Education, School of Chemical and Material Engineering, Jiangnan University, Wuxi 214122, PR China.

\*\*\* Corresponding author.

E-mail addresses: [yanlv@dhu.edu.cn](mailto:yanlv@dhu.edu.cn) (Y. Lv), [yue-miao@dhu.edu.cn](mailto:yue-miao@dhu.edu.cn) (Y.-E. Miao), [txliu@dhu.edu.cn](mailto:txliu@dhu.edu.cn) (T. Liu).

<https://doi.org/10.1016/j.coco.2020.100490>

Received 29 July 2020; Received in revised form 31 August 2020; Accepted 31 August 2020

Available online 12 September 2020

2452-2139/© 2020 Published by Elsevier Ltd.

naphthalene-based polyimide (NPI), nitrogen-doped carbon (NC) and carbon nanotubes (CNT), is denoted as NPI/NC/CNT. Due to the uniform dispersion of NPI within the in-situ formed hierarchical micro/nanoporous conductive network, the NPI/NC/CNT electrode can efficiently inhibit the agglomeration of NPI and enhance the conductivity. Meanwhile, the micro/nanopores within the composite nanofibers can increase the interfacial contact area between the electroactive material and electrolyte, thus contributing to improved utilization of the electroactive C=O groups. As a result, the NPI/NC/CNT electrode delivers a high reversible capacity of  $111.5 \text{ mA h g}^{-1}$  at  $50 \text{ mA g}^{-1}$ , good rate capability of  $39 \text{ mA h g}^{-1}$  at  $2000 \text{ mA g}^{-1}$  and excellent cycling stability of  $89.2 \text{ mA h g}^{-1}$  after 500 cycles as a binder-free cathode for SIBs, which are much higher than those of previously reported organic electrodes as listed in Table S1. Therefore, reasonable construction of NPI/NC/CNT composite nanofibrous membrane can provide new strategies for developing high-performance flexible electrodes in energy storage fields.

## 2. Experimental

### 2.1. Materials

1,4,5,8-naphthalenetetracarboxylic dianhydride (NTCDA) and *p*-phenylenediamine (PDA) were obtained from TCI, Tokyo Chemical Industry Co., Ltd, Tokyo, Japan. Polyacrylonitrile (PAN,  $M_w = 86000$ ), polymethyl methacrylate (PMMA,  $M_w = 350000$ ), *N,N*-dimethylformamide (DMF, 99.9%) were purchased from Sigma Aldrich. Multi-walled carbon nanotubes (MWCNT, 10–20 nm in diameter and 10–30  $\mu\text{m}$  in length) were supplied by Chengdu Institute of Organic Chemistry, Chinese Academy of Sciences, China. All of the reagents were analytical grade and used without further purification.

### 2.2. Fabrication of NPI/NC/CNT and NPI/NC/CNT-powder

CNT was first surface-modified by a mixture of  $\text{H}_2\text{SO}_4/\text{HNO}_3$  (3/1, v/v) [26]. Then, 0.4 g of CNT was dispersed in 20.0 g of DMF by sonication in a 40 kHz ultrasonic bath for 10 h. Equal molar amounts of NTCDA (2.6818 g, 0.01 mol), PDA (1.0814 g, 0.01 mol) and 31.5 g of DMF were mixed in a 250 mL round-bottom flask equipped with a mechanical stirrer under Ar atmosphere, followed by intense mechanical stirring at  $120^\circ\text{C}$  for 12 h. After the reaction, a viscous polymer solution was obtained and sealed under  $0^\circ\text{C}$ , which was signed as NPAA. Subsequently, 8.12 g of the NPAA polymer solution, 1.5 g of PMMA and 0.35 g of PAN were added into the above 10.0 g of CNT dispersion solution under Ar atmosphere and magnetically stirred at  $0^\circ\text{C}$  for another 12 h to obtain the NPAA/PAN/PMMA/CNT dispersion solution, which was then electrospun into nanofiber membrane by applying an electrical potential of 15 kV. For in-situ thermal imidization of NPAA and different degrees of decomposition of PAN and PMMA, the as-obtained nanofiber membrane was dried at  $80^\circ\text{C}$  in a vacuum oven and followed by heat-treated at  $400^\circ\text{C}$  under Ar for another 2 h to obtain the NPI/NC/CNT membrane. For comparison, the NPI/NC/CNT-powder electrode was prepared via the coating method. Typically, the NPAA/PAN/PMMA/CNT dispersion solution was cast onto an aluminum current collector using a doctor blade. Then, the NPI/NC/CNT-powder was obtained using a heat treatment process similar to that of the nanofiber membrane before battery assembly.

### 2.3. Characterizations

Morphologies of NPAA/PAN/PMMA/CNT and NPI/NC/CNT nanofiber membranes were observed using a field-emission scanning electron microscope (FESEM, HitachiS-8010, Japan) and transmission electron microscope (TEM, Talos F200S, Thermo Fisher, USA). The chemical

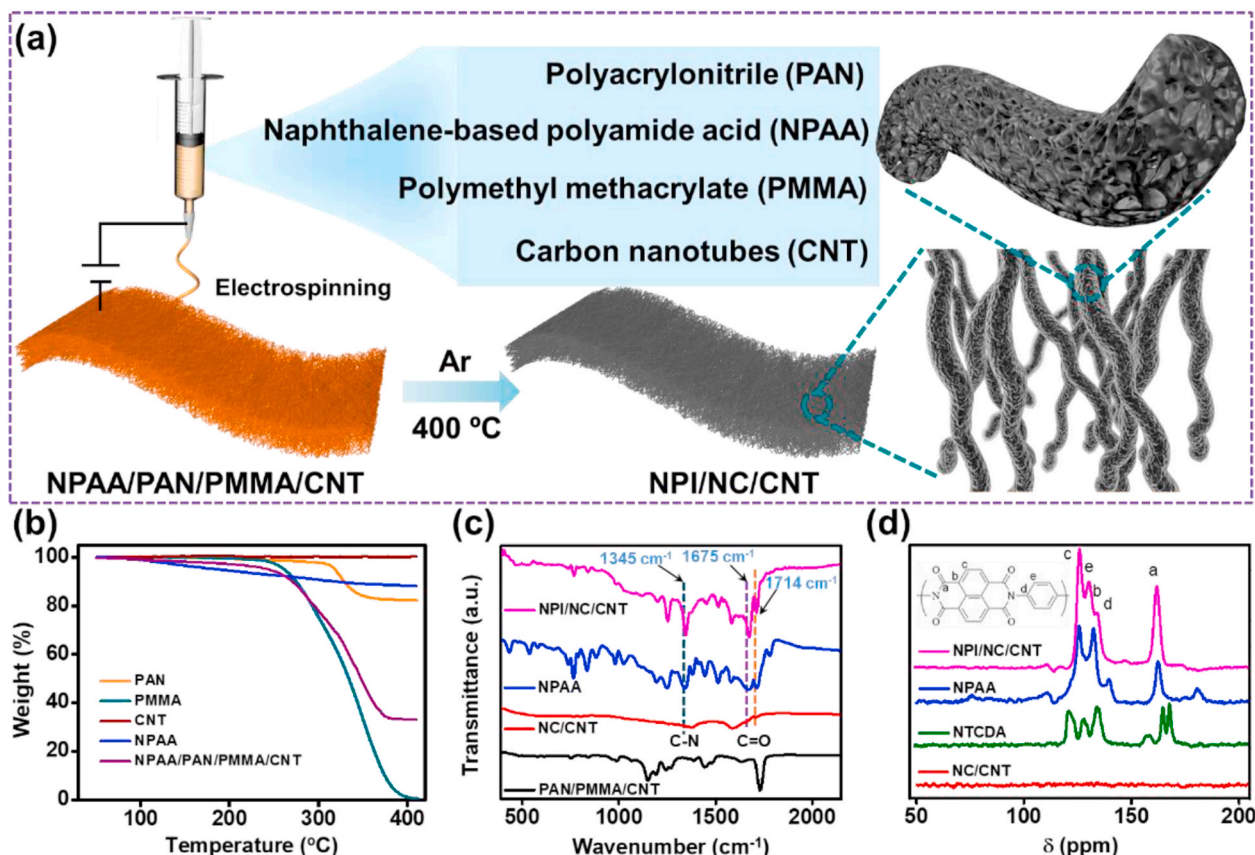


Fig. 1. (a) Schematic illustration for the preparation of NPI/NC/CNT nanofiber membrane. (b) TGA curves, (c) FTIR and (d)  $^{13}\text{C}$  NMR spectra of different samples.

structures and compositions of the samples were characterized by Fourier transform infrared (FTIR, NicoletIn10MX/Nicolet 6700, Thermo Fisher, USA),  $^{13}\text{C}$  nuclear magnetic resonance ( $^{13}\text{C}$  NMR, BrukerAvance 400, Switzerland), and thermogravimetric analyzer (TGA, NETZSCH TG 209 F1 Libra®, Germany) with a temperature ramp of  $10\text{ }^\circ\text{C min}^{-1}$  under  $\text{N}_2$  atmosphere, respectively. Brunauer-Emmett-Teller (BET) surface area ( $S_{\text{BET}}$ ) of the NPI/NC/CNT nanofiber membrane and NPI/NC/CNT-powder were determined by an ASAP 2020 analyzer based on the nitrogen adsorption-desorption isotherms and pore width distribution was also calculated based on a Barrette-Joynere-Halenda (BJH) model. Mechanical property of the NPI/NC/CNT nanofiber membrane was measured by a universal testing machine (SANS, Shenzhen, China) at a tensile speed of  $5\text{ mm min}^{-1}$ . Electrical conductivity of the NPI/NC/CNT nanofiber membrane was measured by a four-point probes resistivity measurement system (RST-8 model, Guangzhou four-point probe technology Co., LTD, China).

#### 2.4. Electrochemical tests

The NPI/NC/CNT nanofiber membrane was cut into round slices with a diameter of 12 mm and directly used as the binder-free electrodes to assemble CR2032 coin-type batteries. For SIBs, a metallic sodium foil was used as the counter electrode, 1 M  $\text{NaClO}_4$  in EC:DMC (1:1, v/v) with 5.0% FEC as the electrolyte, and a glass fiber (Whatman) as the separator. All of the batteries were assembled in an argon-filled glove box with moisture and oxygen content below 0.1 ppm. The galvanostatic discharge/charge experiments and cyclic voltammetry (CV) tests were conducted on a battery-testing system (Land CT-2001A, Wuhan, China) and an Arbin Instruments testing system (Arbin-SCTS, USA), respectively. Electrochemical impedance spectroscopy (EIS, 0.01 Hz-100 kHz, 5 mV) measurements were performed on an electrochemical workstation (CHI 760D, China).

#### 2.5. Calculations

The sodium-ion apparent diffusion coefficient values ( $D$ ) can be calculated from the CV test using the Randles-Sevcik Equation (1) [27, 28]:

$$i_p = 2.69 \times 10^5 n^3 S D^{1/2} C V^{1/2} \quad (1)$$

where  $i_p$  is the peak current (A),  $n$  is the number of transferred electrons,  $D$  is the diffusion coefficient of  $\text{Na}^+$  ( $\text{cm}^2 \text{s}^{-1}$ ),  $S$  is the surface area of the electrode,  $C$  is the concentration of electrolyte, and  $V$  is the potential scan rate ( $\text{V s}^{-1}$ ).

### 3. Results and discussions

As analyzed by the TGA results (Fig. 1b), NPI/NC/CNT composite membrane is obtained through the thermal imidization of naphthalene-based polyamide acid (NPAA) derived from the polymerization of NTCDA and *p*-phenylenediamine (PDA), accompanying with the decomposition of polyacrylonitrile (PAN) and polymethyl methacrylate (PMMA) at  $400\text{ }^\circ\text{C}$ . Meanwhile, hierarchical micro/nanoporous structure is created inside the NPI/NC/CNT composite nanofibers, which will be beneficial for  $\text{Na}^+$  transport and increase the contact area between NPI and electrolyte. The chemical composition of NPI/NC/CNT was determined by Fourier transform infrared (FTIR) spectroscopy and  $^{13}\text{C}$  nuclear magnetic resonance ( $^{13}\text{C}$  NMR) spectroscopy. As shown in Fig. 1c, the characteristic vibration absorption peaks observed at  $1714\text{ cm}^{-1}$ ,  $1675\text{ cm}^{-1}$  and  $1345\text{ cm}^{-1}$  are assigned to the imide  $\text{C}=\text{O}$  and  $\text{C}-\text{N}$  bonds, respectively. In contrast, there is no stretching vibration peak for NC/CNT in the FTIR spectrum. Additionally,  $^{13}\text{C}$  NMR spectroscopy of NPI/NC/CNT indicates the conjugated carbonyl groups from imide rings of NPI at 162 ppm and aromatic carbon of phenyl or naphthalene in the range of 125–147.5 ppm (Fig. 1d), respectively,

further confirming the formation of NPI.

The morphology and structure of NPAA/PAN/PMMA/CNT and NPI/NC/CNT composite nanofiber membranes were investigated using field-emission scanning electron microscopy (FESEM) and transmission electron microscopy (TEM). The NPAA/PAN/PMMA/CNT composite forms a three-dimensional (3D) interwoven network structure with uniform fiber diameter around  $1\text{ }\mu\text{m}$  (Fig. S1a). Besides, carbon nanotubes are uniformly dispersed and embedded in the single nanofiber of NPAA/PAN/PMMA/CNT (Fig. S1b). After heat treatment at  $400\text{ }^\circ\text{C}$ , the as-obtained NPI/NC/CNT nanofiber membrane well maintains the 3D framework with an overall thickness around  $75\text{ }\mu\text{m}$  (Fig. 2a, Figs. S1c and S1d). Moreover, the NPI/NC/CNT single nanofiber shows interconnected micro/nanoporous structure with pore size ranging from a few nanometers to hundreds of nanometers, while CNT is evenly embedded in the micro/nanoporous structure as shown in Fig. 2b–d. Furthermore, the energy dispersive spectroscopy (EDS) mappings reveal very homogenous distribution of NPI within the composite nanofibers (Fig. 2e). As a result, the NPI/NC/CNT nanofiber membrane well inherits the original flexibility of 85.7% elongation at break and good shape retention even after 100 bending cycles (Fig. 2f). Additionally, benefitting from the interconnected conductive skeleton, the NPI/NC/CNT nanofiber membrane also holds a rather high in-plane conductivity of  $0.421\text{ S cm}^{-1}$  after 100 bending cycles, which indicates great potential in serving as a flexible cathode without binders and conductive additives (Fig. 2g). With the unique hierarchical micro/nanoporous structure of a single nanofiber, the NPI/NC/CNT nanofiber membrane further exhibits a high specific surface area of  $121.6\text{ m}^2 \text{ g}^{-1}$  and large pore volume of  $4.638\text{ cm}^3 \text{ g}^{-1}$  in comparison with NPI/NC/CNT-powder (Fig. 2h and i).

The electrochemical properties of NPI/NC/CNT nanofiber membrane for sodium storage were evaluated using 1 M  $\text{NaClO}_4$  in ethylene carbonate/dimethyl carbonate (1:1, v/v) as the electrolyte with 5.0% fluoroethylene carbonate. The typical cyclic voltammetry (CV) curves exhibit two pairs of redox peaks at 2.26 V and 2.16 V, 2.07 V and 1.92 V versus  $\text{Na}^+/\text{Na}$  (Fig. 3a), corresponding to the reversible formation of radical anion intermediates in the redox processes [25]. In addition, the subsequent CV cycles show stable redox peaks with highly overlapped profiles, indicating an excellent stability of NPI/NC/CNT during cycling. The charge/discharge profiles in Fig. 3b exhibit serial voltage plateaus in the first five cycles of NPI/NC/CNT nanofiber cathode at 50 mA g $^{-1}$ , further demonstrating the reversible formation of the radical anion (NPI $^-$ ) and radical dianion (NPI $^{2-}$ ) in the redox processes due to chemical bond reaction mechanisms between NPI and Na as illustrated in Fig. 3c [21,29]. The NPI/NC/CNT cathode demonstrates excellent rate performance with steady reversible capacities of 98, 83.5, 69, 55, 39 mA h g $^{-1}$  at 100, 200, 500, 1000 and 2000 mA g $^{-1}$ , respectively (Fig. 3d). Meanwhile, the cathode can easily recover its initial capacity even after cycling at a high current density of 2000 mA g $^{-1}$ , indicating the low polarization and efficient utilization of NPI. Furthermore, the NPI/NC/CNT cathode delivers an ultrahigh discharge capacity of 103.5 mA h g $^{-1}$  at 200 mA g $^{-1}$ , and slightly decreases to 89.2 mA h g $^{-1}$  after 500 cycles with a high Coulombic efficiency of 100% as displayed in Fig. 3e. In sharp contrast, the NPI/NC/CNT-powder electrode exhibits a rather low initial discharge capacity of 29.5 mA h g $^{-1}$  and poor cycling performance (Fig. S2) due to the agglomeration and poor conductivity of NPI/NC/CNT-powder (Fig. S3).

The excellent electrochemical properties of NPI/NC/CNT are not only determined by its stable molecular structure, but also depend on the reaction kinetics. CV measurements at various scan rates from 0.1 to  $0.5\text{ mV s}^{-1}$  were performed to investigate the advantages of NPI/NC/CNT toward the sodium storage (Fig. 4a). As displayed in Fig. 4b, the peak currents ( $i_p$ ) are proportional to the square root of the scan rate ( $\nu^{0.5}$ ) according to CV curves at different scan rates. Thus, based on the Randles-Sevcik equation (calculation details in Supplementary Information), a much higher diffusion coefficient ( $1.19 \times 10^{-12}\text{ cm}^2 \text{ s}^{-1}$ ) of  $\text{Na}^+$  can be obtained for compared to those of previously reported results

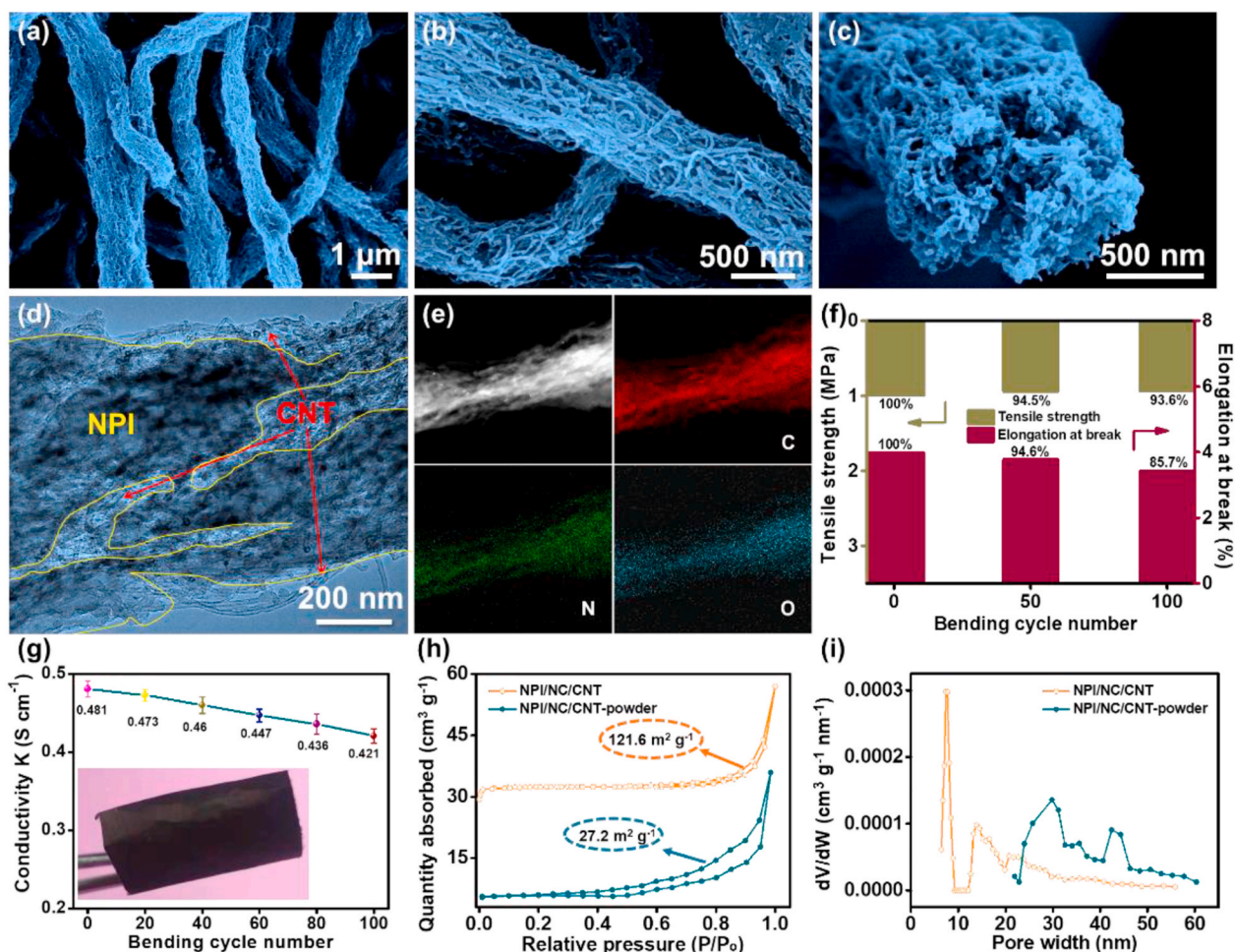


**Fig. 2.** Characterizations of the NPI/NC/CNT nanofiber membrane: (a–c) SEM, (d) TEM, and (e) the corresponding elemental mappings. (f) Mechanical properties and (g) electrical conductivity after different bending cycles. The inset in (g) indicates the flexibility of the nanofiber membrane. (h)  $N_2$  adsorption-desorption isotherms and (i) pore size distribution of the NPI/NC/CNT nanofiber membrane and NPI/NC/CNT-powder, respectively.

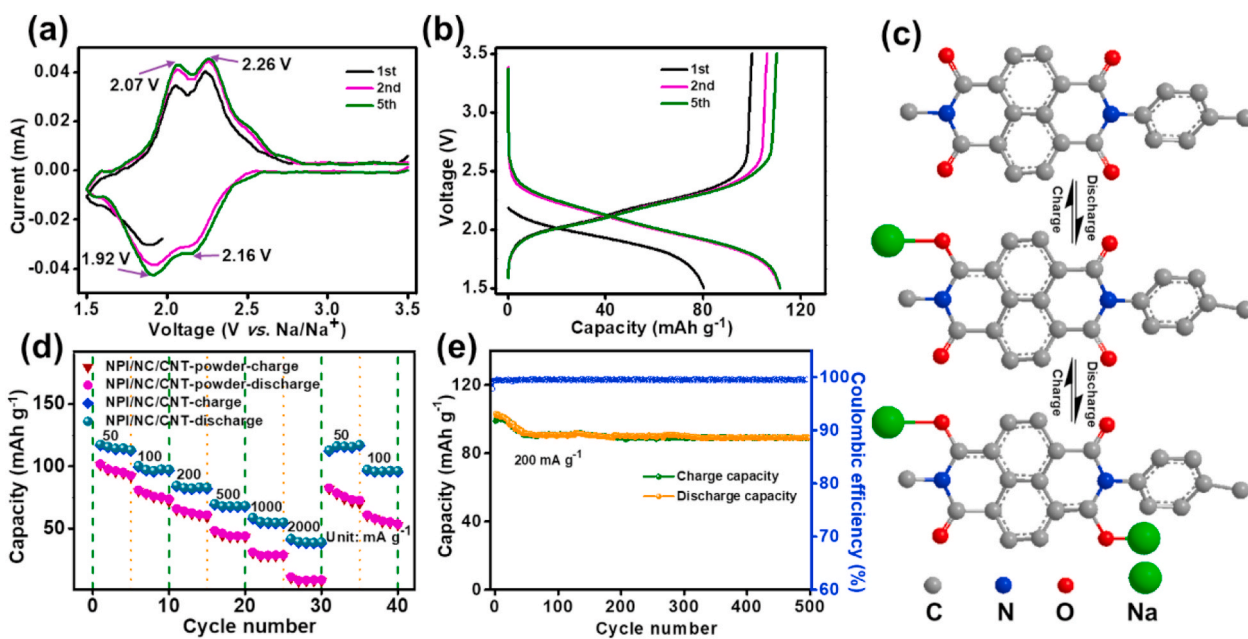


**Fig. 3.** Electrochemical performances of the NPI/NC/CNT cathode in SIBs: (a) CV curves at a scan rate of  $0.1 \text{ mV s}^{-1}$ , (b) charge/discharge voltage profiles at a current density of  $50 \text{ mA g}^{-1}$ , (c) possible redox mechanisms between NPI and Na, (d) rate performance, and (e) cycling stability at a current density of  $200 \text{ mA g}^{-1}$ .

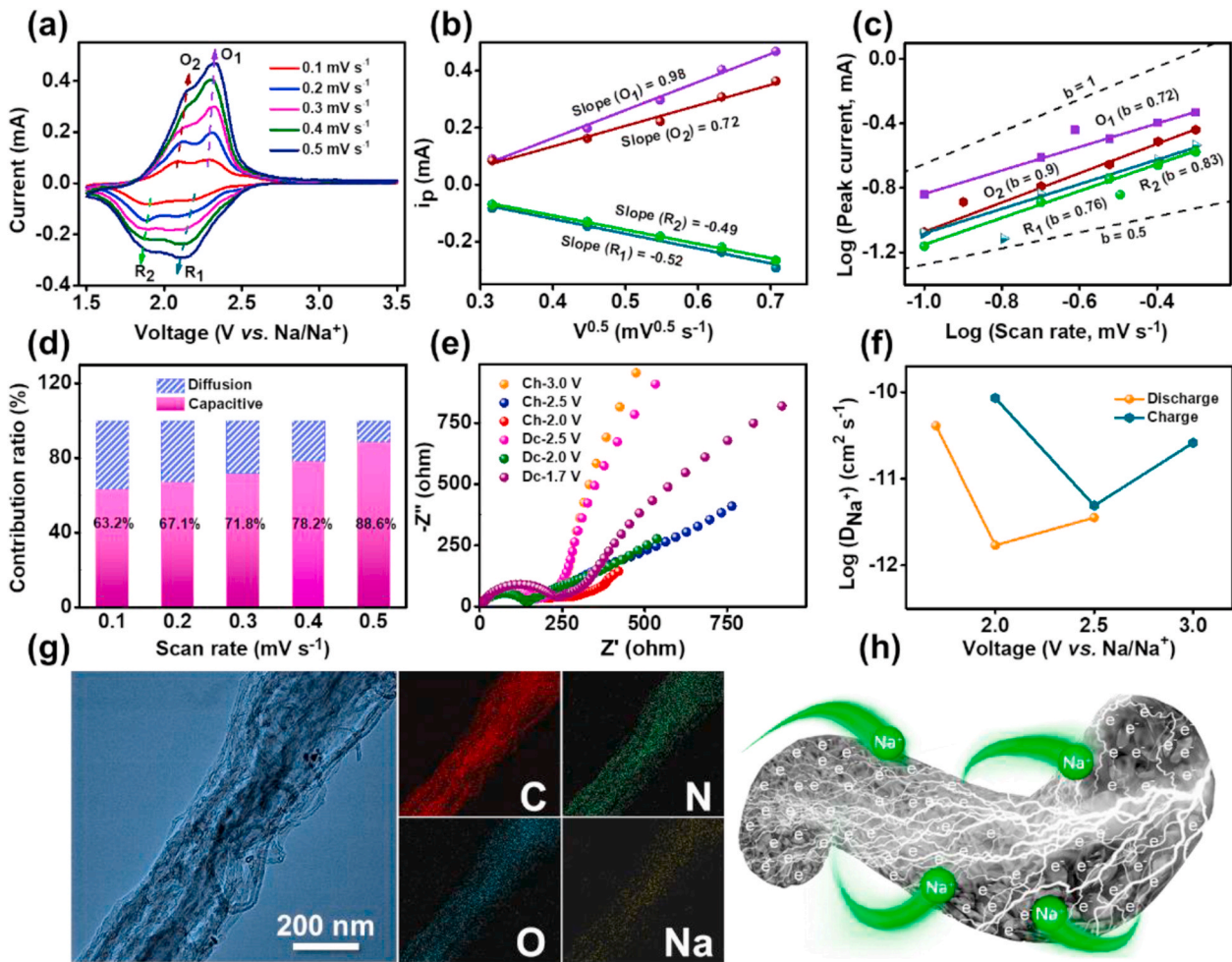


**Fig. 4.** Electrochemical mechanisms of the NPI/NC/CNT cathode in SIBs: (a) CV curves, (b) linear relationship between the peak current ( $i_p$ ) and the square root of scan rates ( $v^{1/2}$ ), (c)  $b$ -values analysis, (d) normalized contribution ratios at different scan rates, (e) Nyquist plots and (f) calculated diffusion coefficients of  $\text{Na}^+$  at different discharge/charge states. (g) *Ex-situ* TEM images and corresponding EDS mappings of C, N, O and Na after 500 cycles. (h) Schematic of the fast electron transport and ion diffusion in the interconnected micro/nanoporous conductive architecture.

as listed in Table S2, demonstrating rapid  $\text{Na}^+$  transport property. Additionally, the reaction kinetics were further estimated based on the relationship between peak current ( $i$ ) and voltage scan rate ( $v$ ), which can be expressed by the following formulae:

$$i = av^b \quad (2)$$

$$\log(i) = b \times \log(v) + \log(a) \quad (3)$$

where  $i$  and  $v$  are the peak current and scan rate, respectively, and  $a$  and  $b$  are the adjustable parameters. In theory, the  $b$  value approaches 0.5 for a diffusion-controlled process, while  $b$  value of 1 represents a surface capacitance-dominated process. As shown in Fig. 4c, according to the linear relationship between  $\log(i)$  versus  $\log(v)$  plots, the  $b$  values of the four redox peaks are calculated as 0.76, 0.83 and 0.72, 0.9, respectively, implying that the capacity of NPI/NC/CNT is contributed by both the diffusion-controlled and capacitive processes. The contribution ratios can be calculated according to the following equations:

$$i(V) = k_1 v + k_2 v^{1/2} \quad (4)$$

$$i(V) / v^{1/2} = k_1 v^{1/2} + k_2 \quad (5)$$

where  $k_1 v$  and  $k_2 v^{1/2}$  represent the capacitive-controlled current and

diffusion-limited current at a particular voltage. Both the parameters of  $k_1$  and  $k_2$  are determined from the linear relationship of  $i(V)/v^{1/2}$  and  $v^{1/2}$  based on equation (5). As shown in Fig. 4d, the contribution ratio of the capacitive processes at different scan rates is in the range of 63.2–88.6%. The high proportions of surface capacitive contribution are ascribed to the fast reaction kinetics due to the interconnected micro/nanoporous conductive skeleton and homogenous distribution of NPI within the whole electrode.

The ion diffusion and charge transfer kinetics during cycling were evaluated by electrochemical impedance spectroscopy (EIS) under an open circuit condition at different discharge/charge states. As shown in Fig. 4e, all Nyquist plots display a small semicircle at high frequency and a sloping line in the low frequency region. The small semicircle at high frequency range indicates low charge-transfer resistance at the NPI/NC/CNT/electrolyte interface, while the straight sloping line in the low frequency region corresponds to the diffusion resistance of  $\text{Na}^+$  within NPI/NC/CNT cathode [25]. The diffusion coefficients of  $\text{Na}^+$  ( $D_{\text{EIS}}$ ) can be calculated at different discharge/charge states based on the following equation [25,30]:

$$D_{\text{EIS}} = \frac{R^2 T^2}{2S^2 n^4 F^4 C^2 \delta^2} \quad (6)$$

where  $R$  is the gas constant ( $8.314 \text{ J mol}^{-1} \text{ K}^{-1}$ ),  $T$  is the absolute temperature (K),  $S$  is the contact area of the electrode,  $n$  is the number of

electrons per molecule,  $F$  is the Faraday constant ( $96486 \text{ C mol}^{-1}$ ),  $C$  is the concentration of  $\text{Na}^+$  and  $\delta$  is the Warburg coefficient. The  $\sigma$  values can be obtained from the slope of  $Z'$  versus  $\omega^{-0.5}$  plots in the Warburg region under different discharge/charge states (Fig. S4). As shown in Fig. 4f, the high  $D_{EIS}$  values are in the range from  $10^{-12}$  to  $10^{-10} \text{ cm}^2 \text{ S}^{-1}$  according to equation (6), further confirming the rapid  $\text{Na}^+$  transport in NPI/NC/CNT cathode. Besides, the morphology of NPI/NC/CNT cathode after 500 cycles at  $200 \text{ mA g}^{-1}$  in SIBs was investigated by TEM (Fig. 4g). Remarkably, no obvious morphological changes are observed after 500 cycles compared with that of the original NPI/NC/CNT. Meanwhile, abundant C, N, O and Na elements can be observed obviously and evenly dispersed in whole NPI/NC/CNT nanofiber, further confirming the excellent structural stability. These high diffusion coefficients of  $\text{Na}^+$  and excellent electrochemical properties manifest fast reaction kinetics and efficient utilization of NPI in NPI/NC/CNT cathode, which are attributed to the well-designed interconnected micro/nanoporous conductive architecture in NPI/NC/CNT nanofiber as described in Fig. 4h.

#### 4. Conclusions

In summary, we have designed and fabricated naphthalene-based polyimide composite nanofibers with hierarchical micro/nanoporous structures and interconnected conductive networks for high-performance organic cathode in SIBs. Due to the 3D interwoven nanofiber network structure and interconnected conductive skeleton, the obtained NPI/NC/CNT composite nanofiber membrane exhibits excellent mechanical flexibility and high in-plane conductivity, which can achieve ultrafast  $\text{Na}^+$  diffusion and electron transfer during discharge/charge processes, thereby leading to high efficient utilization of NPI and ultrafast reaction kinetics in SIBs. Consequently, the NPI/NC/CNT cathode delivers high reversible capacity, superior rate performance and long cycle life for SIBs. Besides, the postmortem studies further reveal the superior mechanical durability and perfect combination of different components. Therefore, the novel design of micro/nanoporous naphthalene-based polyimide composite nanofibers may provide new opportunities for the development of green and sustainable organic electrode materials.

#### CRedit authorship contribution statement

**Gangyong Zhou:** Conceptualization, Methodology, Investigation, Formal analysis, Data curation, Visualization, Writing - original draft, Writing - review & editing. **Lulu Mo:** Investigation. **Chunyang Zhou:** Investigation. **Yan Lv:** Investigation. **Yue-E. Miao:** Writing - review & editing, Supervision, Funding acquisition. **Tianxi Liu:** Writing - review & editing, Supervision, Funding acquisition.

#### Declaration of competing interest

The authors declare that they have no known competing financial interests or personal relationships that could have appeared to influence the work reported in this paper.

#### Acknowledgements

The authors are grateful for the financial support from the Natural Science Foundation of Shanghai (18ZR1401600), "Chenguang Program" supported by Shanghai Education Development Foundation and Shanghai Municipal Education Commission (16CG39), the Shanghai Scientific and Technological Innovation Project (18JC1410600), and the Fundamental Research Funds for the Central Universities and Graduate Student Innovation Fund of Donghua University (CUSF-DH-D-2019006).

#### Appendix A. Supplementary data

Supplementary data to this article can be found online at <https://doi.org/10.1016/j.coco.2020.100490>.

A flexible naphthalene-based polyimide/nitrogen-doped carbon/carbon nanotubes (NPI/NC/CNT) composite nanofiber membrane with hierarchical micro/nanoporous structure and interconnected conductive frameworks is reasonably designed for organic sodium-ion batteries. The NPI/NC/CNT cathode exhibits long cycling stability and excellent rate capability.

#### References

- [1] Y. Fang, X.Y. Yu, X.W. Lou, Nanostructured electrode materials for advanced sodium-ion batteries, *Matter* 1 (2019) 90–114.
- [2] F. Xie, L. Zhang, Q. Gu, D. Chao, M. Jaroniec, S.Z. Qiao, Multi-shell hollow structured  $\text{Sb}_2\text{S}_3$  for sodium-ion batteries with enhanced energy density, *Nanomater.* Energy 60 (2019) 591–599.
- [3] T. Zhu, P. Hu, X. Wang, Z. Liu, W. Luo, K.A. Owusu, W. Cao, C. Shi, J. Li, L. Zhou, L. Mai, Realizing three-electron redox reactions in NASICON-structured  $\text{Na}_3\text{MnTi}(\text{PO}_4)_3$  for sodium-ion batteries, *Adv. Energy Mater.* 9 (2019), 1803436.
- [4] Y. Yan, Z. Ma, H. Lin, K. Rui, Q. Zhang, Q. Wang, M. Du, D. Li, Y. Zhang, J. Zhu, W. Huang, Hydrogel self-templated synthesis of  $\text{Na}_3\text{V}_2(\text{PO}_4)_3$ @C/CNT porous network as ultrastable cathode for sodium-ion batteries, *Compos. Commun.* 13 (2019) 97–102.
- [5] W. Li, S. Hu, X. Luo, Z. Li, X. Sun, M. Li, F. Liu, Y. Yu, Confined amorphous red phosphorus in MOF-derived N-doped microporous carbon as a superior anode for sodium-ion battery, *Adv. Mater.* 29 (2017), 1605820.
- [6] Y. Zhang, S. Ullah, G.P. Zheng, X.C. Zheng, D. Li, Advanced sodium storage properties of a porous nitrogen-doped carbon with a  $\text{NiO}/\text{Cu}/\text{Cu}_2\text{O}$  hetero-interface derived from bimetal-organic frameworks, *Chem. Commun.* 56 (2020) 818–821.
- [7] H. Wu, X. Zhang, Q. Wu, Y. Han, X. Wu, P. Ji, M. Zhou, G. Diao, M. Chen, Confined growth of 2D  $\text{MoS}_2$  nanosheets in N-doped pearl necklace-like structured carbon nanofibers with boosted lithium and sodium storage performance, *Chem. Commun.* 56 (2019) 141–144.
- [8] J.J. Tian, H. Yang, C.M. Fu, M.L. Sun, L.N. Wang, T.X. Liu, In-situ synthesis of microspherical  $\text{Sb}@C$  composite anode with high tap density for lithium/sodium-ion batteries, *Compos. Commun.* 17 (2020) 177–181.
- [9] J. Fei, Y. Cui, J. Li, Z. Xu, J. Yang, R. Wang, Y. Cheng, J. Hang, A flexible  $\text{Sb}_2\text{O}_3/\text{carbon}$  cloth composite as a free-standing high performance anode for sodium ion batteries, *Chem. Commun.* 53 (2017) 13165–13167.
- [10] R. Kunwar, M. Harilal, S.G. Krishnan, B. Pal, I.I. Misnon, C.R. Mariappan, F. I. Ezema, H.I. Elim, C.C. Yang, R. Jose, Pseudocapacitive charge storage in thin nanobelts, *Adv. Fiber. Mater.* 1 (2019) 205–213.
- [11] S.M. Tang, Z.T. Liu, C. Jiang, Y.C. Wu, H.Y. Li, B. Wang, E. Wang, J. Ma, C.L. Wang, Tailoring p-conjugated systems: from p-p stacking to high-rate-performance organic cathodes, *Inside Chem.* 4 (2018) 2600.
- [12] S. Gu, S. Wu, L. Cao, M. Li, N. Qin, J. Zhu, Z. Wang, Y. Li, Z. Li, J. Chen, Z. Lu, Tunable redox chemistry and stability of radical intermediates in 2D covalent organic frameworks for high performance sodium ion batteries, *J. Am. Chem. Soc.* 141 (2019) 9623–9628.
- [13] Y. Wu, Y. Chen, M. Tang, S. Zhu, C. Jiang, S. Zhuo, C. Wang, A highly conductive conjugated coordination polymer for fast-charge sodium-ion batteries: reconsidering its structures, *Chem. Commun.* 55 (2019) 10856–10859.
- [14] T. Liu, Y. Zhang, Z. Jiang, X. Zeng, J. Ji, Z. Li, X. Gao, M. Sun, Z. Lin, M. Ling, J. Zheng, C. Liang, Exploring competitive features of stationary sodium ion batteries for electrochemical energy storage, *Energy Environ. Sci.* 12 (2019) 1512–1533.
- [15] Z. Zhu, H. Li, J. Liang, Z. Tao, J. Chen, The disodium salt of 2,5-dihydroxy-1,4-benzoquinone as anode material for rechargeable sodium ion batteries, *Chem. Commun.* 51 (2015) 1446–1449.
- [16] H. Zhu, J. Yin, X. Zhao, C. Wang, X. Yang, Humic acid as promising organic anodes for lithium/sodium ion batteries, *Chem. Commun.* 51 (2015) 14708–14711.
- [17] Q. Zhao, Y. Lu, J. Chen, Advanced organic electrode materials for rechargeable sodium-ion batteries, *Adv. Energy Mater.* 7 (2017), 1601792.
- [18] J. Li, M. Luo, Z. Ba, Z. Wang, L. Chen, Y. Li, M. Li, H.B. Li, J. Dong, X. Zhao, Q. Zhang, Hierarchical multicarbonyl polyimide architectures as promising anode active materials for high-performance lithium/sodium ion batteries, *J. Mater. Chem.* 7 (2019) 19112–19119.
- [19] S. Lei, X. Cui, X. Liu, X. Zhang, X. Han, Y. Yang, Hydrothermally self-templated synthesis of rectangular polyimide submicrotubes and promising potentials in electrochemical energy storage, *Chem. Commun.* 56 (2020) 1429–1432.
- [20] C. Chen, X. Zhao, H.B. Li, F. Gan, J. Zhang, J. Dong, Q. Zhang, Naphthalene-based polyimide derivatives as organic electrode materials for lithium-ion batteries, *Electrochim. Acta* 229 (2017) 387–395.
- [21] H. Peng, S. Wang, M. Kim, J. Kim, Y. Yamauchi, J. Yu, D. Li, Highly reversible electrochemical reaction of insoluble 3D nanoporous polyquinoneimines with stable cycle and rate performance, *Energy Storage Mater.* 25 (2020) 313–323.
- [22] F. Xu, H. Wang, J. Lin, X. Luo, S. Cao, H. Yang, Poly(anthraquinonyl imide) as a high capacity organic cathode material for Na-ion batteries, *J. Mater. Chem.* 4 (2016) 11491–11497.

- [23] J. Wang, F. Li, Y. Qu, Y. Liu, Y. Yang, W. Li, M. Zhao, PNTCDA: a promising versatile organic electrode material for alkali-metal ion batteries, *J. Mater. Chem.* 6 (2018) 24869–24876.
- [24] J. Xie, Q. Zhang, Synthesis and exploration of ladder-structured large aromatic dianhydrides as organic cathodes for rechargeable lithium-ion batteries, *Chem. Asian J.* 12 (2017) 868–876.
- [25] G.Y. Zhou, Y.E. Miao, Z.X. Wei, L.L. Mo, F.L. Lai, Y. Wu, J.M. Ma, T.X. Liu, Bioinspired micro/nanofluidic ion transport channels for organic cathodes in high-rate and ultrastable lithium/sodium-ion batteries, *Adv. Funct. Mater.* 28 (2018) 1804629.
- [26] J. Liu, A.G. Rinzler, H. Dai, J.H. Hafner, R.K. Bradley, P.J. Boul, A. Lu, T. Iverson, K. Shelimov, C.B. Huffman, Fullerene pipes, *Science* 280 (1998) 1253–1256.
- [27] Y. Lu, S. Zhang, Y. Li, L. Xue, G. Xu, X. Zhang, Preparation and characterization of carbon-coated NaVPO<sub>4</sub>F as cathode material for rechargeable sodium-ion batteries, *J. Power Sources* 247 (2014) 770–777.
- [28] T. Yang, T. Qian, M. Wang, X. Shen, N. Xu, Z. Sun, C. Yan, A sustainable route from biomass byproduct okara to high content nitrogen-doped carbon sheets for efficient sodium ion batteries, *Adv. Mater.* 28 (2016) 539–545.
- [29] Z. Ba, Z. Wang, M. Luo, H.B. Li, Y. Li, T. Huang, J. Dong, Q. Zhang, X. Zhao, Benzoquinone-based polyimide derivatives as high-capacity and stable organic cathodes for lithium-ion batteries, *ACS Appl. Mater. Interfaces* 12 (2020) 807–817.
- [30] L. Li, X. Tang, H. Liu, Y. Qu, Z. Lu, Morphological solution for enhancement of electrochemical kinetic performance of LiFePO<sub>4</sub>, *Electrochim. Acta* 56 (2010) 995–999.